JOURNAL OF MATERIALS SCIENCE 20 (1985) 77–84

Material and geometry effects on crack shape in double torsion testing

P. S. LEEVERS, J. G. WILLIAMS
Department of Mechanical Engineering, Imperial College of Science & Technology, London SW7 2BX, UK

Previous work has established a model for expressing the curved crack front shape observed in a Double Torsion test in a single parameter, the shape factor S. This paper demonstrates the ability of this model to account for crack shape effects on measured toughness against crack speed data, using a direct measurement of S, in tests on polymethyl methyacrylate (PMMA) of various molecular weights. The analysis is then extended to enable S to be predicted without reference to the material crack front size parameter referred to in earlier work: only specimen geometry significantly influences the crack front shape in a wide variety of materials.

1. Introduction

A typical problem in basic Fracture Mechanics research is the evaluation of *crack resistance* as a function $R(\dot{\xi})$ of *crack speed*, whose influence can reveal the nature of separation processes in the material [1] or of transport mechanisms in its environment [2]. R is the work, W, absorbed at a locally-straight section $\delta\eta$ of advancing crack front:

$$R \equiv \frac{1}{\delta\eta}\left(\frac{dW}{d\xi}\right) \quad (1)$$

ξ being a coordinate fixed in the crack plane and directed normally to η. Several test methods can provide an observable image of $R(\dot{\xi})$ as $G_c(\dot{a})$, where $\dot{a}$ is the *crack velocity* in a specific direction, measured directly or – for an elastic body – calculated as

$$\dot{a} = \frac{\dot{v}}{P_c(dC/da) + C(dP_c/da)} \quad (2)$$

Here load, P_c, and load-point displacement, v, are observed during crack extension; the crack path width, B_c, is measured; and compliance, $C \equiv v/P_c$, and *strain energy release rate*

$$G_c = \frac{P_c^2}{2B_c}\left(\frac{dC}{da}\right) \quad (3)$$

are calculated.

In the Tapered Double Cantilever Beam (TDCB) specimen, the crack front is quite straight, $\dot{\xi} \simeq \dot{a}$, as observed along a surface, and little distortion of the $R(\dot{\xi}) \rightarrow G_c(\dot{a})$ mapping is to be expected. Its use, however, may be complicated by crack wandering, or breakage or yield of the arms near the loading points; furthermore, the contouring process itself can prove expensive. The Double Torsion (DT) test (Fig. 1), by contrast, seems extremely simple, using a rectangular plate, and is generally less sensitive to crack wandering. The complexities here, however, are interpretative, and arise from the markedly curved crack front.

The DT compliance function $C(a)$ can be measured directly, or estimated by elastic analysis – assuming simple torsion over the separated length, a, of each rectangular-section arm, and an unchanging torsional compliance at its root. Hence

$$\frac{dC}{da} = \frac{(1+\nu)}{E}\frac{D^2}{ZHB^3} \quad (4)$$

where geometric parameters are defined in Fig. 1, Z is a tabulated function of (B/H), and E and ν are the elastic modulus and Poisson's ratio. The established accuracy of Equation 4 validates these assumptions about the outer deformation field, which imply that the separated crack surfaces are split apart on one specimen face and forced

0022–2461/85 $03.00 + .12

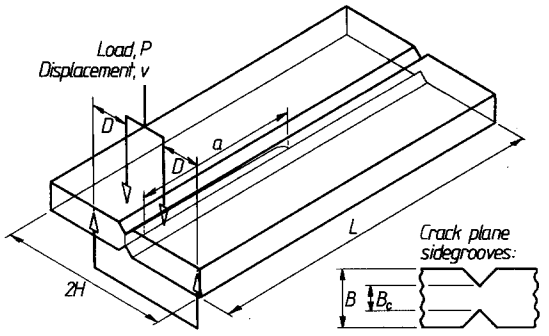

Figure 1 The Double Torsion test.

together on the other, "touching" only at a unique neutral axis, NA.

To resolve this physically implausible picture, further assumptions must be made:

(i) The advancing crack front follows a contour of constant face separation as extrapolated inwards from this assumed deformation field, and, simultaneously,

(ii) in-plane beam flexure takes place so that the NA shifts to a position midway across the still-unseparated width of the crack path.

This deformation model is complete, and proves [3, 4] to provide an accurate prediction of the crack front shape:

$$b = B_c\left(\frac{S}{S+y^*}\right) \tag{5}$$

where $x = b$ is the uncracked path width (the ligament) at $y^* \equiv (a-y)/B_c$. This shape, which translates with a, and can be recorded instantaneously on the exposed surface (e.g. by sudden arrest, or a discontinuity in crack velocity), is uniquely characterized by its dimensionless *shape factor*, S, measurable via a simple geometric construction (Fig. 2). In terms of the assumed deformation field, SB_c is the distance beyond $y = a$ at which the torsion beam twist extrapolates to zero. It can also be shown that, according to

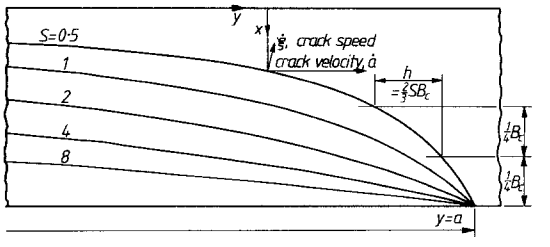

Figure 2 Calculated DT crack shapes for a typical range of observed shape factors, S.

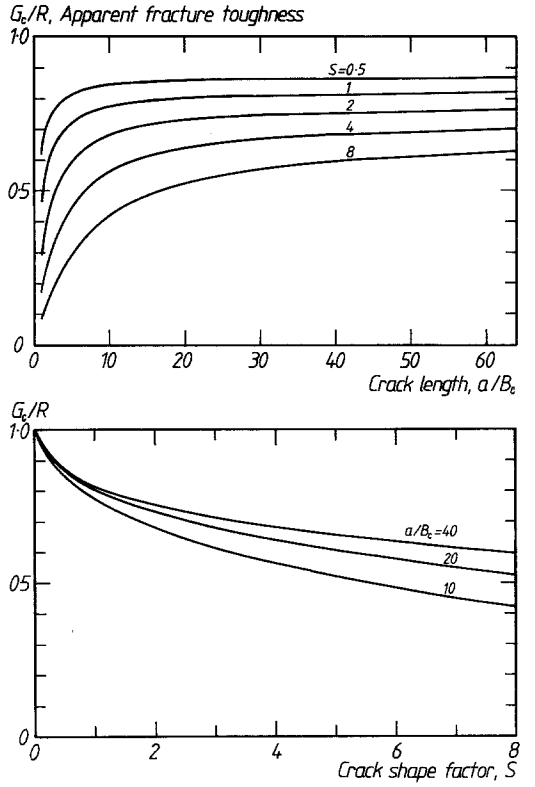

Figure 3 Predicted crack length and shape effects on DT test toughness results, for a power-law rate-dependent material ($n = 0.1$).

Equation 5 and assumption (ii), the beam *flexure* extrapolates linearly to zero at the crack tip, implying a local, concentrated couple there, and no net crack plane surface tractions elsewhere.

Crack front curvature re-emphasizes the distinction between crack speed and velocity, and thus between $R(\dot{\xi})$, a postulated material property, and $G_c(\dot{a})$, its observable image, averaged from R along the front. Using the DT crack shape model, this can be made explicit [3]:

$$G_c(\dot{a}) = \int_{S/(S+a/B_c)}^{1} R\left[\dot{a}x^{*2}/(S^2+x^{*4})^{\frac{1}{2}}\right] \mathrm{d}x^* \tag{6}$$

For many materials, $R(\dot{\xi})$ approximates to an exponential form

$$R = R_1\dot{\xi}^n \tag{7}$$

with R_1 a constant; e.g. for PMMA in air, $n \simeq 0.1$ for crack speeds of some μm sec^{-1} to some mm sec^{-1} [5]. Then, Equation 6 becomes

$$\frac{G_c(\dot{a})}{R(\dot{a})} = \int_{S/(S+a/B_c)}^{1} \frac{x^{*2n}}{(S^2+x^{*4})^{n/2}}\,\mathrm{d}x^* \tag{8}$$

Integrating the dummy variable out of Equation 8 for $n = 0.1$ (Fig. 3) suggests that:

(a) a pronounced (for high S) crack length effect is caused by the increasing proportion of available path width, B_c, within which the crack front is actually propagating (a thin ligament of material may still hold the specimen together even after fracture), and

(b) even for long cracks, gross errors in estimating R from G may be made if the disparity between front speed and translation velocity is not accounted for.

The objects of the work described here were twofold. Firstly (Section 2), we aim to demonstrate that DT tests actually induce these expected disparities between G and R, and that they can be corrected for using a *measured* value of the shape factor, S. Secondly, our understanding of the factors controlling crack shape is tested by attempting to *predict* S for a particular test. Some further analysis of the beam root deformation system allows S to be expressed as a function of geometry, and this is evaluated using data from a range of different materials.

2. Crack shape effects on G_c against $\dot{a}$ data

Fig. 3 predicts that S will have a pronounced effect on G_c against $\dot{a}$ data for PMMA ($n \simeq 0.1$), and Stalder and Kausch [4] have already demonstrated the influence of plate thickness and sidegroove depth on S (or, in their notation, MF_1). Adopting, in a modified form, the experimental techniques of Stadler and Kausch, we tested larger ($2H =$ 90 mm) DT specimens of ICI Perspex PMMA, under a range of controlled crosshead rates on a 100 kN Instron machine – to yield crack translation velocities spanning more than a decade around 1 mm sec^{-1}. Crack length was recorded on the load–displacement trace to provide an individual compliance calibration, $C(a)$, for each test. While the crack was propagating steadily near the half-width point ($a > 10B_c$), the crosshead was suddenly driven into fast reverse ($\dot{v} = 1$ m min^{-1}) to unload the specimen, which was then inverted and fractured at the same rate. The exposed surface, a crack front arrest line clearly marked on it as a boundary between distinct textures, was then metallized and photographed to × 12 magnification, and S was calculated from two measurements (Fig. 2) as

$$S = \frac{3}{2}\frac{h}{B_c} \qquad (9)$$

Whilst the in-plane specimen size was held constant (90 mm × 180 mm), thickness and sidegroove depth were varied: 6 mm thick specimens were grooved to 1.5 mm depth (as for earlier tests on polyesters [3]) or left ungrooved, 10 mm thick specimens grooved to 1, 1.5, 2, 2.5, 3 and 3.5 mm depth. Ironically – crack path stabilization being the main purpose of DT specimen sidegrooving – only tests on the latter, deepest-grooved geometry were aborted due to crack wandering. With insufficient rigidity in the uncracked section to react against torsional end loading, these specimens behaved like elongated four-point bend types, the crack tearing raggedly and discontinuously up from several initiation points on the tension surface. Cracks in ungrooved specimens merely curved gently from the centreline, suffering no change in section thickness and showing only a slight departure from linearity in $C(a)$.

The expected crack-length effect on apparent toughness (Fig. 3) emerges most clearly in deeply-grooved 10 mm specimens; the rising load traversed a broad maximum as the support compliance of the ligament rose. Plotting $G_c(\dot{a})$ data as calculated from Equations 2 and 3 for each specimen shows (Fig. 4) scatter of about ± 25%, but there is a systematic tendency for more deeply grooved specimens to yield lower apparent toughness values. If this arises from crack shape effects, the most accurate data should originate from ungrooved 6 mm and 1 mm grooved 10 mm specimens. These do indeed constitute an upper bound, and regression analysis on the form of Equation 8 yields $n = 0.08$ and 0.11, respectively, in good agreement with earlier results [1].

Correcting each result from Equation 8, using $n = 0.1$, achieves a dramatic reduction in scatter (Fig. 5): ± 5% limits provide a 90% confidence band around a characteristic with $n = 0.1$ and $R(\dot{\xi} = 1 \text{ mm sec}^{-1}) = 465 \text{ J m}^{-2}$. Although no systematic variation in R with sidegroove depth is now discernible, 6 mm thick material still appears to be tougher than 10 mm material, at low crack speeds, and this may well be a genuine effect. To provide further evidence that this correction procedure reveals a material property characteristic, a second series of tests was carried out, using 6 mm "Perspex" specimens, of number-average molecular weight $\bar{M}_n = 350$k, γ-irradiated to reduce this to various values down to 20k. Crack resistance is thereby reduced, while leaving elastic constants unchanged [6]. Supplementary TDCB tests provided reference data at four values

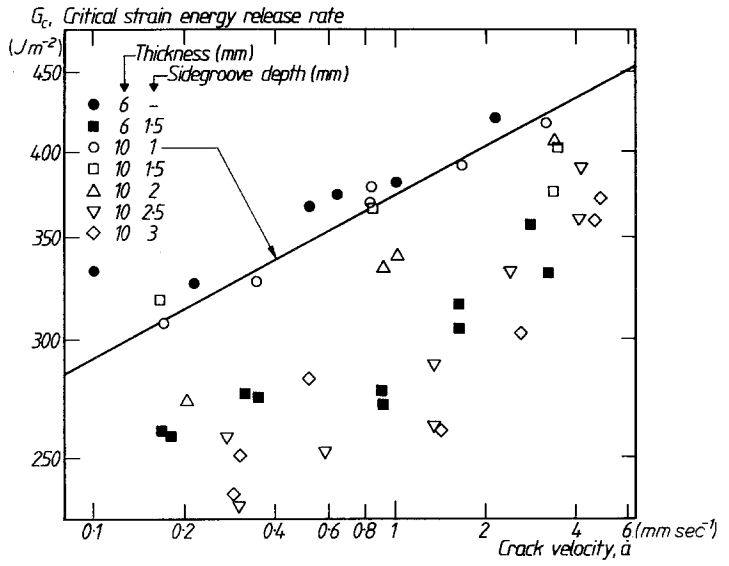

Figure 4 Measured critical strain energy release rate against crack velocity, for PMMA ($\bar{M}_n = 345\,000$) in a range of DT specimen geometries.

of $\bar{M}_n$. Although the crack front in these specimens is essentially straight and orthogonal to the translation direction in the fracture plane, requiring no correction for velocity, it tended to tilt and bow *out* of plane, sometimes leaving a convoluted surface. This effect, which is not significant in DT tests, extends the crack front, and requires a correction to B_c: of up to 10%, measured from Shadowgraph traces, at × 50 magnification, of transverse sections of the crack path.

For each material and geometry, 5 to 10 tests over a range of crosshead speeds allowed G_c ($\dot{a} = 1\,\text{mm sec}^{-1}$) to be accurately and reliably interpolated. For DT data, this interpolation stage was repeated, using the procedure established here to calculate R ($\dot{\xi} = 1\,\text{mm sec}^{-1}$). Fig. 6 shows that this brings close agreement with the $G_c(\dot{a}) = R(\dot{\xi})$ data from TDCB tests – correcting an original under-estimate of up to 40% – and demonstrates the usefulness of the method in pursuit of a particular goal. The irradiated materials show a toughness plateau to extend down to $\bar{M}_n = 40$k, with a precipitous fall below this value; a possible explanation has been discussed elsewhere [6].

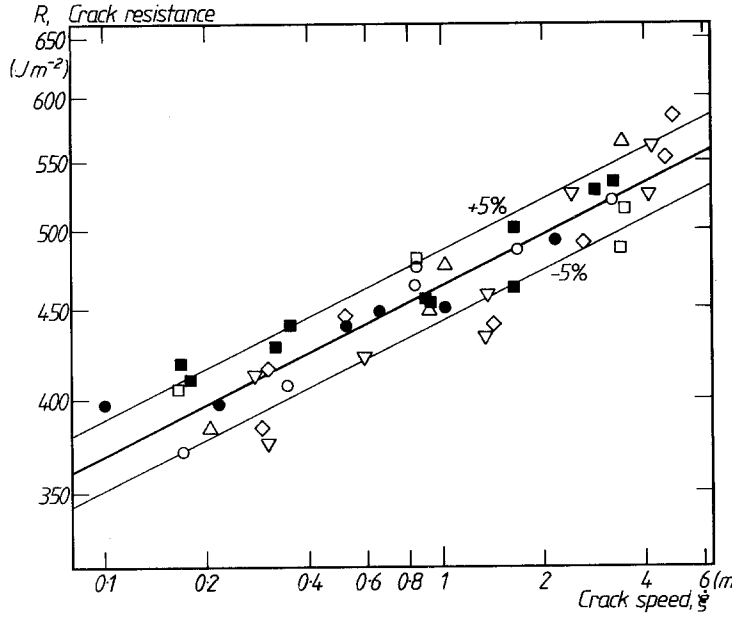

Figure 5 Corrected crack resistance against crack speed characteristic for PMMA, from data of Fig. 4.

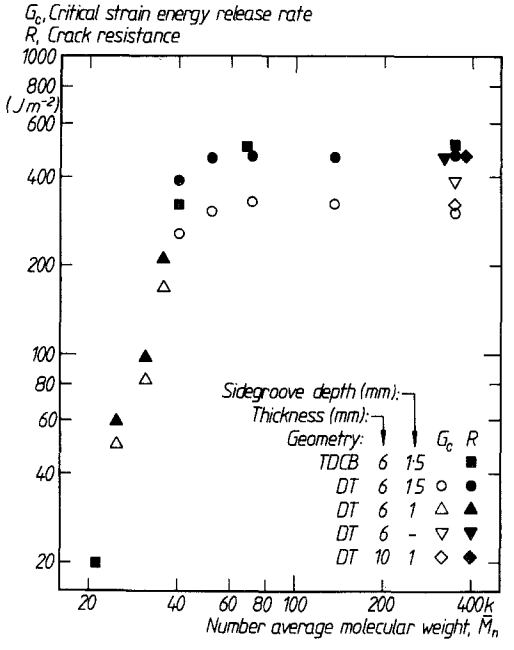

Figure 6 Measured (G_c) and corrected (R) crack resistance, from DT tests on PMMA of various molecular weights at a crack speed of 1 mm sec^{-1}.

3. Geometry effects on crack shape

It has now been demonstrated that Equation 5 describes the DT crack shape very well [3], that this permits a one-parameter description by S, and that, using a *measurement* of S and a calculation scheme based on it, a rate-dependent material property function, $R(\dot{\xi})$, can be distilled from its distorted experimental image, $G_c(\dot{a})$. For practical purposes, it is obviously desirable to be able to *predict* S for a particular test, or at least to understand the influence of geometrical and material property parameters on it, so that shape factor effects can be minimised by design.

To assess the effect of material properties, further DT tests were carried out on materials ranging from polycrystalline alumina, with a vanishingly small crack tip opening displacement (COD), to a titanium alloy with a COD of over 100 μm – fifty times that of PMMA. Thickness and sidegroove depth were varied where possible, but constraints on material availability did not allow any particular geometry to be used for *every* material. Nevertheless, a striking consistency in crack shape across this broad spectrum of properties was observed, as illustrated in Fig. 7 by the front shapes in specimens, having an almost identical geometry (6 mm thick, ungrooved), of glass and of Perspex. In both cases, $S = 0.615$, and the shapes conform very closely indeed to Equation 5. This evidence strongly suggests that δ_f, the postulated constant crack front size, arises only as a component of the outer, elastic displacement field, rather than as any characteristic size of the process zone. This can be established by developing an analysis for geometry effects only, and testing its applicability to all the materials tested.

3.1. Further analysis of the deformation system

Torsion in each rectangular beam is governed by

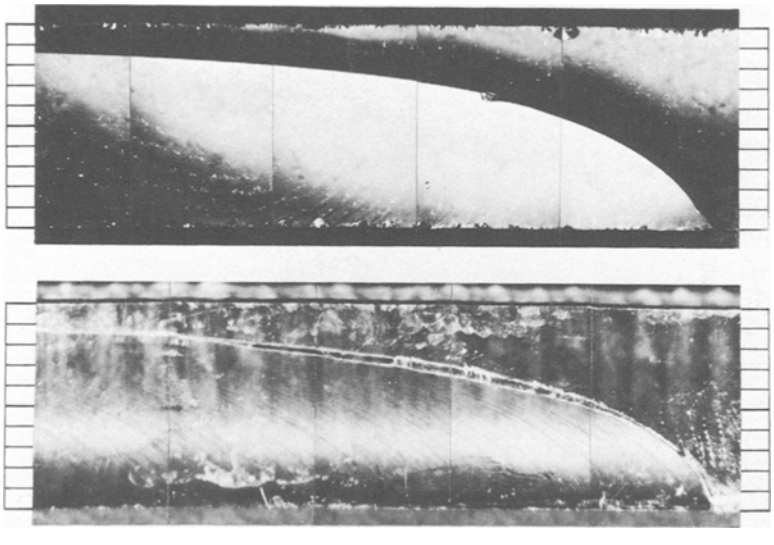

Figure 7 Almost identical crack shapes ($S = 0.61$) in glass (above) and PMMA (below) DT specimens of similar geometry.

the equation

$$M = -\frac{E}{2(1+\nu)} ZHB^3 \frac{d\theta}{dy} \quad (10)$$

where M is the local transmitted moment, and θ is the rotation, in the direction of the applied moment at $y = 0$. Since the torsion $(d\theta/dy)$ is assumed not to decay significantly up to the beam root $y = a$, the entire deformation pattern is fixed by the rotation and torsion at that point. Now S is defined by the extrapolation of the rotation to zero at $y = a + SB_c$ [3]:

$$\theta(a) = SB_c \frac{d\theta}{dy}(a) \quad (11)$$

so that it is independent of the crack front size δ_f, so long as this remains constant over $y < a$. In fact, the rotation will not fall linearly to zero within $a < y < a + SB_c$, since the transmitted moment decays with y, extending the length of moment-supporting structure: this is made obvious in practice by the appearance of finite length effects at $a \ll (L - SB_c)$. A simple "beam on elastic foundation" analysis of the support structure can therefore be used to relate rotation and torsion at the beam root, and thus to predict S.

Because SB_c, characterizing the support deformation region size, is normally much smaller than H, it can be assumed that rigid-section beam torsion continues to dominate any cross-sectional bending. Deformations are therefore localized as displacements normal to the unseparated crack plane surfaces, and are (assuming a mid-plane NA):

$$w(x) = \left(x - \frac{B_c}{2}\right)\theta \quad (12)$$

corresponding to normal tensile tractions $p(x)$. The magnitude of these tractions can be estimated by matching the peak displacement $w(B_c)$ to that at the surface of a semi-infinite elastic plane subjected to a similar array $(p(x), 0 < x < b)$, which is ([5], p. 109):

$$w(b) = -\frac{2}{\pi E} \int_{x=0}^{b} p(x) \ln (b - x)\, dx \quad (13)$$

To apply this result to the crack face problem, we note that, for equilibrium,

$$\int_0^{B_c} p(x) = 0 \quad (14)$$

and incorporate a factor c to account for the increased compliance of a finite crack path width. Integrating Equation 13 by parts then yields:

$$w(B_c) = -\frac{2c}{\pi E} \int_0^{B_c} \frac{\int p(x)\, dx}{(b - x)}\, dx \quad (15)$$

Assuming a linear traction distribution

$$p(x) = p_{max}(2x - B_c)/B_c \quad (16)$$

yields, from (12) and (15):

$$p_{max} = \frac{\pi E}{2c}\theta \quad (17)$$

Since such a distribution exerts a moment per unit length

$$m = -\tfrac{1}{6} p_{max} B_c^2 \quad (18)$$

we arrive at an expression for the decay in applied moment due to absorption by the support:

$$\frac{dM}{dy} = -\frac{\pi E B_c^2}{12c}\theta \quad (19)$$

Differentiating the torsion Equation 10 and substituting Equation 19 yields:

$$\frac{d^2\theta}{dy^2} = \left(\frac{Q}{B_c}\right)^2 \theta \quad (20)$$

where

$$Q \equiv \left[\frac{\pi}{6c}(1+\nu)\frac{B_c^4}{ZHB^3}\right]^{\frac{1}{2}} \quad (21)$$

A solution with $\theta(a)$ imposed and incorporating the finite-length boundary condition:

$$\frac{d\theta}{dy} = 0 \text{ at } y = L \text{ (no transmitted moment)} \quad (22)$$

is

$$\theta(y) = \theta(a)\frac{\cosh [Q(L - y)/B_c]}{\cosh [Q(L - a)/B_c]} \quad (23)$$

Thus, Equation 11 becomes

$$S = \frac{1}{Q}\coth [Q(L - a)/B_c] \quad (24)$$

This appears to constitute the sought-for prediction of S once the factor c in Equation 21, which must bear the burden of our various noted assumptions, has somehow been estimated. A method for doing so emerges if it is noted that the load-point compliance of each beam support:

$$C_o \equiv \frac{v}{P} = \frac{D^2}{2}\frac{\theta(a)}{M} \quad (25)$$

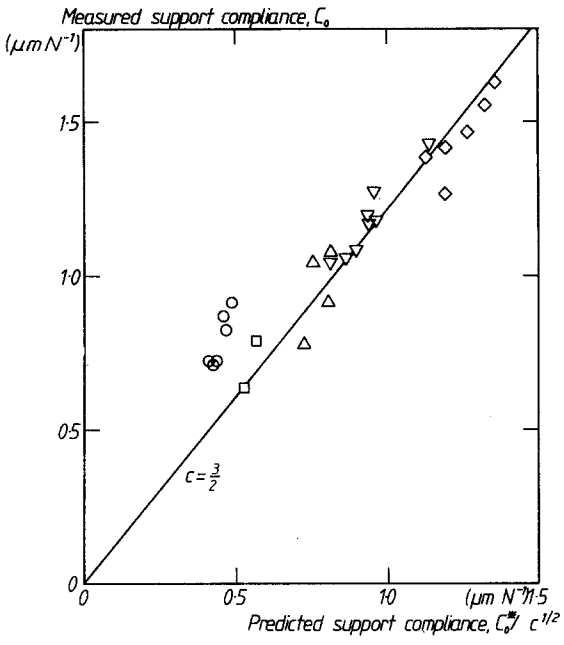

Figure 8 Measured against predicted beam support compliance, from DT tests on PMMA (see Fig. 4 for key).

is predicted to be, via Equation 10, 11 and 24:

$$C_o = C_o^* \coth\left[\frac{Q(L-a)}{B_c}\right] \quad (26)$$

where

$$C_o^* \equiv \frac{D^2}{EB_c}\left[\frac{6c}{\pi}\frac{(1+\nu)}{ZHB^3}\right]^{\frac{1}{2}} \quad (27)$$

For a sufficiently deep support, the hyperbolic finite-length correction is unity, and c can be estimated by plotting C_o (as extrapolated from the $C(a)$ characteristic for each specimen at moderate crack lengths) against $C_o^*/c^{1/2}$.

3.2. Comparison with experimental results

Using data from the series of variable-geometry DT tests on PMMA, the modulus was calculated using an expression

$$E = E_1\dot{v}^{0.04} \quad (28)$$

inferred from Equation 4 by plotting (dC/da), as measured, against the geometric term. The constant E_1 was evaluated by three-point bending tests on DT specimen halves using corresponding centre displacement rates: $E_1 = 2.7$ GPa, at $\dot{v} = 1$ mm min^{-1}. Z was calculated using an interpolation polynomial:

$$Z = \frac{1}{3} - 0.24\left(\frac{B}{H}\right) + 0.13\left(\frac{B}{H}\right)^2 \quad (29)$$

to express the values tabulated in [5].

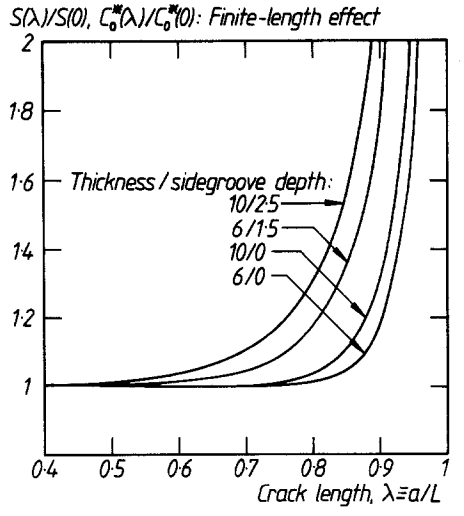

Figure 9 Finite-length effects on crack shape factor and beam support compliance for various DT geometries.

The resulting plot of C_o against C_o^* (Fig. 8) shows $c = 1.5$ to be a reasonable approximation, although scatter and divergence from linearity are too great to support the proposed model as a complete picture of the beam–root deformation system. Beyond such sources of scatter as uncertainties in the extrapolation of $C(a)$ to C_o, there are signals of more systematic effects. Shallow sidegrooves (lower C_o values) imply c values of up to 3; although greater compliance would be expected from the lack of support on the crack path edge, this value is too great to be physically plausible. However, Fig. 9, which shows the finite-length effects on crack shape and root compliance to be expected for $c = 1.5$, seems to under-estimate those actually observed [3], again suggesting a higher c value than much of the data in Fig. 8 imply.

Turning to the formal structure of the shape factor prediction using Equations 21 and 24 provides more encouragement (Fig. 10). In the region of greatest practical interest ($S < 4$), the S data from variable sidegroove and thickness tests on Perspex (Fig. 10a) differ from those predicted only by a constant factor. Beyond this region, S tends to exceed the predicted value, but it is under these circumstances that the appearance of isolated crack initiation points ahead of the crack tip on the tension surface, and a general associated raggedness of the crack front, subvert *any* shape prediction. Measured S data for the other materials tested (Fig. 10b) show a looser overall correlation, suggesting some material dependence of the

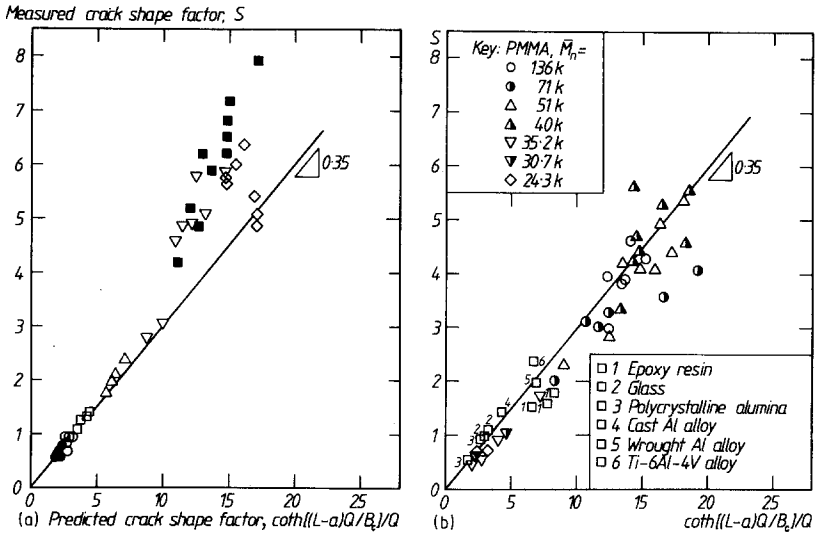

Figure 10 Crack shape factor as measured against that predicted from specimen geometry only: (a) PMMA, $\bar{M}_n$ = 345 000 (see Fig. 4 for key), (b) other materials.

unexplained scale factor relating predicted and observed shape factors.

It must now be pointed out that tractions binding the crack plane faces together, which have been accounted for in this analysis only ahead of the tip, will inevitably exert a significant moment behind the tip as well. Pursuit of this idea through to a complete analysis of the crack shape, again assuming a constant crack tip face separation, δ_f, is relatively straightforward, but leads only to a point at which δ_f must be *evaluated*, defeating the intention to provide an S prediction useful to the materials technologist. For such purposes, as illustrated in Section 2, an adequate estimate is given by:

$$S = 0.35Q' \coth [(L-a)/Q'B_c] \quad (30)$$

where

$$Q' = 2\left(\frac{B}{B_c}\right)^2 \left[\frac{ZH}{\pi(1+\nu)B}\right]^{\frac{1}{2}} \quad (31)$$

Clearly, in order to minimize S, it is better to avoid thin materials, and to cut sidegrooves as shallow as possible – if at all.

The ever-increasing accessibility of cheap computing power must be taken into account when selecting a materials testing technique. So simple and convenient is the Double Torsion test as a method of fracture toughness testing – particularly for rate-sensitive materials – that the computing effort required to foresee and correct for crack shape effects is insignificant by comparison. Even if a direct evaluation of S is necessary to achieve the required accuracy with greater reliability than Equations 30 and 31 can predict, it is, in most materials, easily made.

4. Conclusions

1. G_c against $\dot{a}$ data from Double Torsion tests should be corrected by a factor derived from a measurement of the crack front shape, in order to achieve an adequate approximation to the underlying material property. This is particularly important for the rate-dependent materials, typified here by PMMA.

2. The crack front shape can be characterized by a single parameter, the shape factor S, which can be predicted, with an accuracy adequate for general purposes, from the specimen geometry only.

3. For specimens of a given size, the shape factor and its effects can be minimized by avoiding the use of thin materials and by keeping sidegrooves, if they are necessary, as shallow as possible.

References

1. G. P. MARSHALL, L. H. COUTTS and J. G. WILLIAMS, *J. Mater. Sci.* 9 (1974) 1409.
2. M. K. V. CHAN and J. G. WILLIAMS, *Polymer* **24** (1983) 234.
3. P. S. LEEVERS, *J. Mater. Sci.* **17** (1982) 2469.
4. B. STALDER and H. H. KAUSCH, *ibid.* **17** (1982) 2481.
5. S. P. TIMOSHENKO and J. N. GOODIER, "Theory of Elasticity", 3rd edn (McGraw-Hill, New York, 1970).
6. P. PRENTICE, *Polymer* **24** (1983) 344.

Received 10 February
and accepted 29 February 1984